High energy dissipation and self-healing auxetic foam by integrating shear thickening gel

Kang Zhang [a,b,1], Qiang Gao [c,1], Jingchao Jiang [d], Meishan Chan [a,b], Xiaoya Zhai [a,e], Liuchao Jin [a], Jiangfan Zhang [f], Jifan Li [b,**], Wei-Hsin Liao [a,*]

[a] Department of Mechanical and Automation Engineering, The Chinese University of Hong Kong, Hong Kong, China
[b] Nano and Advanced Materials Institute Limited, Hong Kong, China
[c] School of Mechanical Engineering, Southeast University, Nanjing, China
[d] Department of Engineering, University of Exeter, Exeter, EX4 4QF, UK
[e] School of Mathematical Sciences, University of Science and Technology of China, Hefei, China
[f] School of Mechanical Engineering, Nanjing University of Science and Technology, China

ABSTRACT

Herein, we report a novel hybrid auxetic foam (HAF) with high energy dissipation and self-healing properties prepared by integrating shear thickening gel (STG) with auxetic polyurethane foam (APF). Due to the synergetic action of shear thickening property of STG and the negative Poisson's ratio of APF, HAF shows better impact protection performance than APF and PU foam. The quasi-static compression test shows the energy dissipation ability of HAF is around 4 times that of APF. The dynamic impact test demonstrates that the force reduction of HAF increases by as high as 64 %, compared to APF. Notably, the force reduction improvement of the HAF is much higher than other hybrid auxetic materials. It is also found that the peak force of HAF is reduced as the amount of STG increases. Additionally, the peak force difference between HAF and APF becomes larger when they are subjected to higher impact energies, due to the rate-dependent effect of STG inside the foam. The Poisson's ratio results for HAF with different STG content under low and high compression strain rates reveal that the dimension of auxetic cell structures and STG content are required to be carefully designed to maximize the synergistic effect of auxetic property and shear thickening property. Besides, HAF demonstrates self-healing ability, allowing it to repair damage sustained during use and can be assembled like Lego blocks to make structures with any irregular shapes. Our work provides ideas for the development of advanced auxetic materials, with the potential to revolutionize a wide range of applications.

1. Introduction

Energy absorption and impact protection materials are increasingly employed in various domains, including household, transportation, sports, consumer electronics, occupation and military defense, to mitigate personal injuries or damages to valuable goods [1–5]. Among the flexible impact protection materials, foam is widely utilized due to its effectiveness in dissipating impact energy through the buckling and collapse of its pore structures [6–8]. Researchers have found that incorporating auxetic structures into foam leads to improved energy absorption performance [9–13]. In conventional foam, the material at the impact site tends to flow away upon being hit by an object, resulting in decreased density of the foam. Conversely, in foam with auxetic structure, the material tends to flow towards the impact side, increasing foam density and enabling it to absorb more impact energy. Despite this densification effect, the energy dissipation capacity of existing auxetic foams remains insufficient, which will hinder their application in fields that require materials to effectively dissipate significant impact energy. Several attempts have been made to improve the impact dissipation performance of auxetic foam. For example, Eunyoung et al. reported a MXene coated auxetic polyurethane foam, which can reduce the peak force by 19.5 % compared to the auxetic foam [14]. Oh et al. studied the

---

energy dissipation of graphene oxide-wrapped auxetic foam. Compared with pristine auxetic foam, the hybrid auxetic foam incorporated with two-dimensional graphene oxide showed 31 % higher in force reduction [15]. Kim et al. tried to coat PLA film with a highly ordered honeycomb concave micropattern on the surface of auxetic foam and found that force reduction of this multi-dimension auxetic foam is improved by 39 % [16]. However, achieving high improvement in energy dissipation performance of auxetic foam is still a challenging. Therefore, it is crucial to develop new approaches to manufacture high-energy-dissipation auxetic foam.

Shear thickening material is a non-Newtonian substance that demonstrates a unique behavior of augmenting its viscosity and stiffness at high shear rates. Shear thickening material has garnered significant attention in recent years due to its potential applications in various fields, including impact protection, body armor, and sports equipment [17–19]. When incorporated into a composite material, shear thickening material can enhance its energy absorption and impact resistance by stiffening upon impact and reducing the transmitted force to the underlying layers [20–25]. Nakonieczna et al. attempted to impregnate auxetic polyester foam with shear thickening fluid (STF) and discovered that the addition of STF to the auxetic foams increased force-absorbing efficiency [26]. However, the liquid state of STF in the auxetic foams leads to leakage problems, rendering it unsuitable for realistic applications. Parisi et al. reported an auxetic polyethylene foam infused with shear thickening gel (STG), but their results indicated that the incorporation of STG caused a marginal reduction in peak impact force, which due to the low and non-uniform levels of STG infusion in the close-cell structures of auxetic polyethylene foam [27]. To date, the development of auxetic foam with STG to achieve high energy dissipation has not been reported.

Foam materials with self-healing properties represent a significant advancement in materials science and engineering due to their ability to repair themselves when damaged, thereby enhancing their durability and lifespan. The technology involved in developing self-healing foam materials includes the incorporation of microcapsules containing healing agents, as well as the use of self-healing polymers such as shape memory materials and reversible chemical bond polymers [28]. While several types of self-healing foam materials, including polyurethane foam, epoxy foam, silicone foam, and ethylene-vinyl acetate foam, have been developed [29–32], the auxetic foam with self-healing property is rarely reported.

In this study, we propose a novel hybrid auxetic foam with high energy dissipation, achieved through the integration of STG with auxetic polyurethane foam (APF). The open pore microstructure of APF facilitates successful penetration of STG through a dipping coating process. The high energy dissipation performance of the resulting hybrid auxetic foam is proved by the quasi-static compression test and the dynamic impact test. The energy dissipation ability of the hybrid auxetic foam is around 4 times that of APF. Compared with APF, the force reduction of hybrid auxetic foam increases by as high as 64 %. The force reduction improvement of the hybrid auxetic foam in this work is much higher than other hybrid auxetic materials reported in literatures. We have systematically studied the effect of STG content, impact energies and compression strain rate on the energy dissipation performance and Poisson's ratio of the hybrid auxetic foam. The results indicate that the energy dissipation performance of hybrid auxetic foam strongly depends on the STG content and the dimension of auxetic cell structures, which will affect the buckling behaviors of cell walls of the foam. Additionally, this paper first reports a hybrid auxetic foam with a self-healing property. The self-healable hybrid auxetic foam can repair damage sustained during use and can be assembled like Lego blocks to make structures with any irregular shapes. These features of the developed hybrid auxetic foam make it a promising candidate for the development of advanced and smart protection materials, with the potential to revolutionize a wide range of industrial and commercial applications.

2. Materials and methods

2.1. Materials

Hydroxyl silicone oil (500 mm^2 s^{-1}, AR degree) and boric acid (99.9 %, Sigma Aldrich) were used to prepare shear thickening gel. Polyurethane (PU) foam (density = 0.016 g/cm^3) was provided by Yong Jia Foam Co., Ltd. Isopropyl alcohol and ethanol were purchased from Sigma Aldrich.

2.2. Synthesis of shear thickening gel

The shear thickening gel (STG) in this paper was a derivative of polyborondimethylsiloxane (PBDMS) and was prepared according to literature [20]. First, boric acid and silicone oil were mixed and stirred uniformly with a mass ratio of 1:20, followed by the mixture being heated in an oven at 180 °C for 2 h. The STG was obtained after cooling the mixture to room temperature.

2.3. Auxetic polyurethane foam preparation

The auxetic polyurethane foam was prepared according to previous work [5]. The original PU foam was put in a home-made aluminum mold with a triaxial compression ratio of 2.9. The mold was then put in an oven for heating at 200 °C for 1 h, and finally cooled down to room temperature to obtain auxetic polyurethane foam (APF). The thickness of the auxetic polyurethane foam is 14 mm.

2.4. Preparation of APF/STG hybrid foam

STG were dissolved in isopropyl alcohol (IPA) medium to make STG/IPA solution. APF was impregnated with this solution. To remove isopropyl alcohol, the samples were heated in an oven at 80 °C overnight. STG contents in the foams were determined with the ratio of STG: IPA. Three different APF/STG composites (APF/2STG, APF/3STG, APF/6STG) have been fabricated. The three samples have different STG content. For example, APF-2STG means that the weight of STG is two times of APF.

2.5. Characterization

The morphology of the PU foam, APF and APF/STG hybrid foam was characterized by SEM (TM3030Plus, Hitachi). The element mapping of APF and APF/STG was acquired using a XFlash660 energy-dispersive EDX detector (Bruker, Germany). A Fourier transform infrared spectrometer (FT-IR, PerkinElmer) was used to characterize the chemical bonding states of the STG through an ATR mode from 4000 to 500 cm^{-1}. The Poisson's ratio measurement was based on video data acquired with a high-speed camera (Qianyan Lang 5F01, Junda Hi-Tech Co., Ltd.) during the quasi-static compression test conducted in the MTS Material Testing System (Model: E43.104). The hysteresis stress–strain curves of the foams were measured by a universal testing machine (LE3104, LiShi (Shanghai) Instruments Co., Ltd.). The specimen size is 20mm × 20 mm × 14 mm for the hysteresis test. The dynamic impact test was carried out by a drop weight tester (L223, LiShi (Shanghai) Instruments Co., Ltd). During the process, the drop hammer weighed 2.5 kg fell from different heights to strike the sample with different impact energy. The surface resilience of the foams was tested according to the DIN 53512 standard using a resilience testing machine (HD-F754, Haida International Equipment Co. Ltd.). DMA (Q800, TA Instrument, USA) was performed at a mechanical dynamic analysis frequency between 0.01 and 100 Hz. The rheological properties were determined using a strain-controlled rheometer (HR20, TA Instrument, USA). Abaqus/Explicit solver was employed for calculation of the deformation. The prototypes for the FE model validation were printed by 3D printer (Raise3D Pro3). For the self-healing performance evaluation, the APF/6STG sample was cut into

two pieces and put together at different temperatures, tensile tests were carried out to determine the tensile strength of sample before and after the self-healing process.

3. Results and discussion

3.1. Fabrication and characterization of APF and APF/STG hybrid foam

The fabrication of APF/STG hybrid foam using a dipping-coating method is schematically shown in Fig. 1a. STG needs to be diluted with organic solvents to decrease its viscosity and thus it can be easily
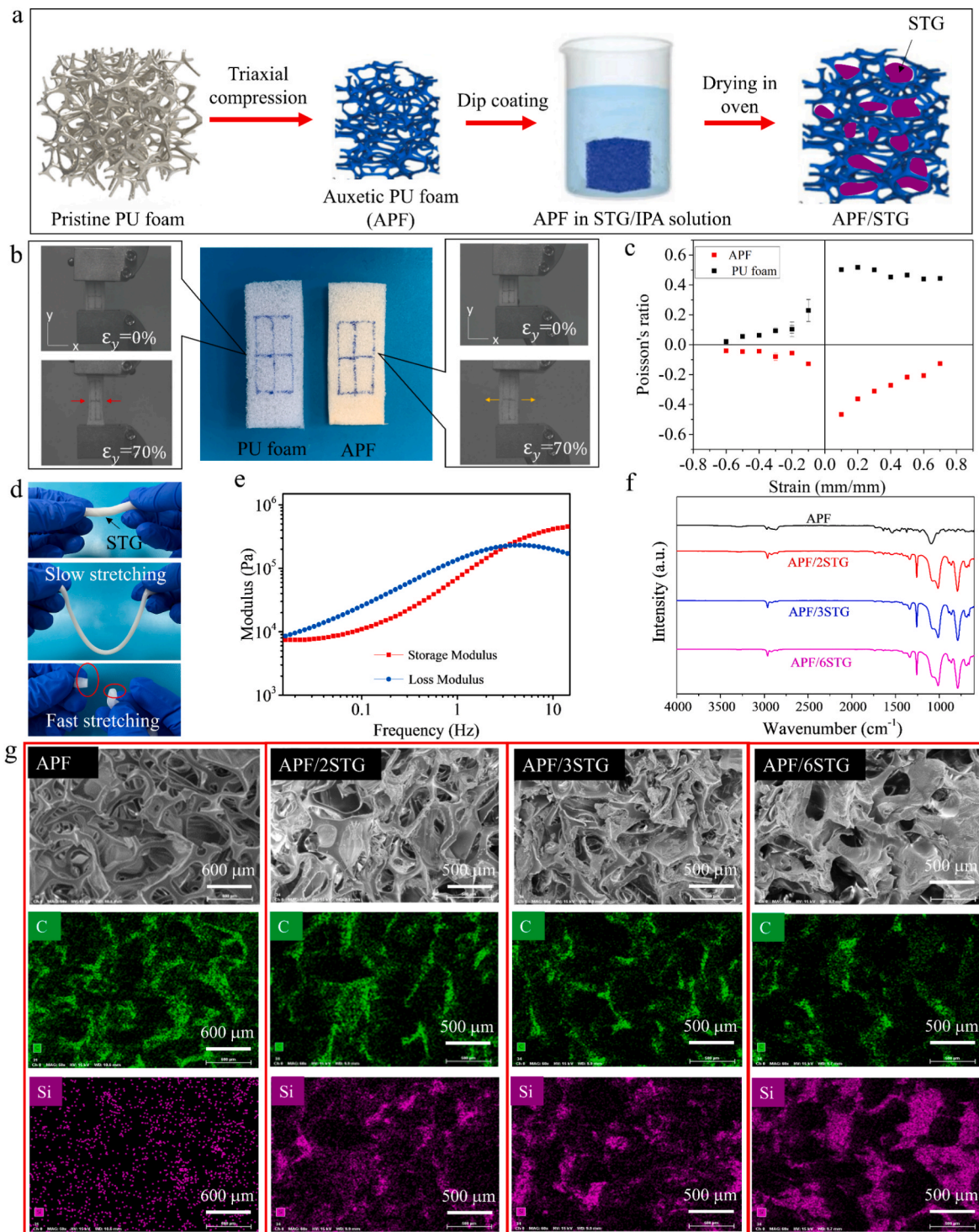

Fig. 1. a) Fabrication schematics of APF/STG hybrid foam. b) Optical images showing the positive Poisson's ratio of PU foam and negative Poisson's ratio of APF. c) Comparison of Poisson's ratio of the pristine PU foam and APF. d) Optical images showing the rate-dependent viscoelastic property of STG. e) Storage modulus and loss modulus of STG as a function of shear frequency ranging from 0.01 to 100 Hz. f) FT-IR spectra of APF, APF/2STG, APF/3STG and APF/6STG (code name: APF/2STG means that the weight of STG is two times of APF). g) SEM and EDX elemental mapping images of APF, APF/2STG, APF/3STG and APF/6STG.

diffused into APF. Micro-computed tomography (μ-CT) provides non-destructive images (Fig. S1) for internal micro-structures of the APF and APF/STG hybrid foam. The thicker thickness of the cell walls of APF/STG hybrid foam in Figs. S1c–e indicates the STG is successfully coated on all skeletons of APF. Fig. 1b shows the picture of PU foam and APF after triaxial thermal compression. The color of sample is changed may be due to the thermal degradation during the high temperature heating process. At 70 % tensile strain, it is found that the width of PU foam becomes smaller while that of APF becomes larger, showing APF has negative Poisson's ratios. Fig. 1c presents the Poisson's ratio as a function of the compression strain and tensile strain for PU foam and APF. The APF exhibits a negative Poisson's ratio as low as - 0.5 and the Poisson's ratio will become larger as the compression strain or tensile strain increases. This finding of the strain-dependent Poisson's ratio of APF agrees well with others [13,33]. Fig. 1d and Fig. S2 show the rate-dependent mechanical behavior of STG. When STG is stretched slowly, it can be easily deformed and displays soft and ductile behavior. However, STG exhibits rigid behavior under fast stretching and shows brittle fracture. Upon rapid compression of STG, the compression strength of the material exhibits a significant increase when compared to that observed at low compression rate. For instance, as depicted in Fig. S2, the compression strength of STG under high compression rate is 0.07 MPa at a compression strain of 0.2, which is approximately 35 times greater than that observed at low compression rate. Fig. 1e is the logarithmic curves of storage modulus and loss modulus of STG at shear frequency increasing from 0.01 to 100 Hz. The storage modulus of STG increases with the increase of shear frequency, revealing that STG has shear-hardening effect. The storage modulus of STG becomes larger than the loss modulus when the shear frequency exceeds the critical value of around 3 Hz, showing the status transition of STG from viscous to elastic. For the FTIR spectroscopy of APF and APF/STG hybrid foam as shown in Fig. 1f, APF/STG hybrid foams (APF/2STG, APF/3STG and APF/6STG) show three additional characteristic absorbance peaks for B–O at 863 cm^{-1}, Si–O–Si at 1009 cm^{-1} and Si–O–B 1340 cm^{-1}, indicating STG exist in the three samples [34,35]. SEM images (Fig. 1g) show that STG is coated on the skeletons of APF. The EDX mapping of chemical elements confirms that three samples (APF/2STG, APF/3STG and APF/6STG) contain silicon elements, which prove that STG is successfully coated on APF. As the STG fraction increases, we can see that the silicon elements areas become larger.

3.2. Mechanical properties and anti-impact performance of APF/STG hybrid foam

The quasi-static compression hysteresis test and dynamic impact test have been used to further evaluate the energy dissipation performance of APF/STG hybrid foam. For the compression hysteresis test, the dissipated energy can be determined by the area enclosed between loading and unloading curves [36]. Fig. 2a shows the stress-strain hysteresis curves of APF and original PU foam. Three repeated tests for each
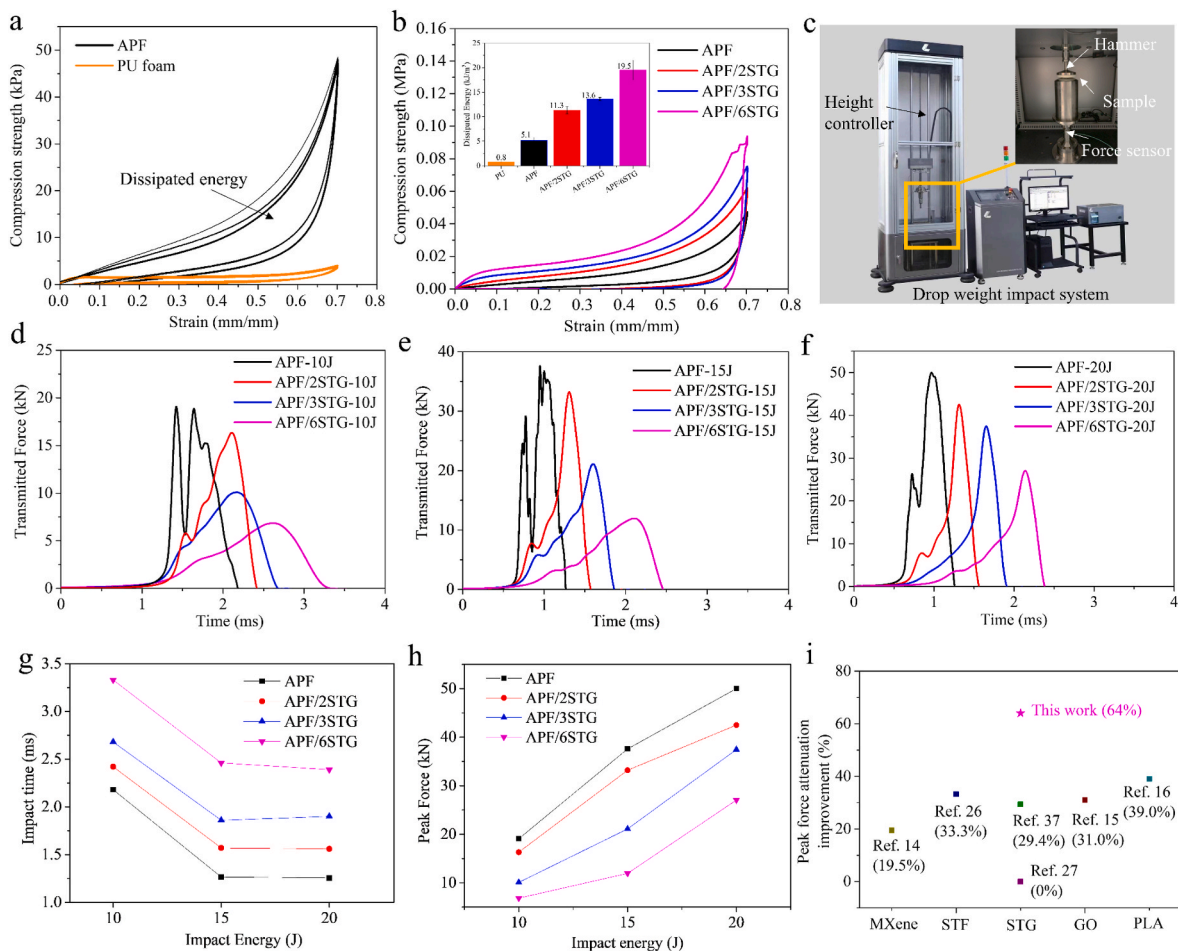

Fig. 2. a) Compressive stress-strain curves of PU foam and APF. b) Compressive stress-strain curves of APF, APF/2STG, APF/3STG and APF/6STG. The inset gives the comparison of energy dissipation of PU foam, APF, APF/2STG, APF/3STG and APF/6STG. c) Drop weight impact test machine. d-f) Transmitted force-time curves of APF, APF/2STG, APF/3STG and APF/6STG under 10 J, 15 J and 20 J, respectively. g) Impact time of APF, APF/2STG, APF/3STG and APF/6STG under 10 J, 15 J and 20 J, respectively. h) Peak force of APF, APF/2STG, APF/3STG and APF/6STG under 10 J, 15 J and 20 J, respectively. i) Comparison of force reduction improvement of hybrid auxetic materials with different functional materials of MXene, STF, STG, GO and PLA.

sample are conducted to ensure the reliability of our experiment. The original PU foam exhibits a classical stress-strain curve with a plateau region under quasi-static compression. However, the stress-strain curve of APF does not show plateau region since the ribs of APF are already curved inward and they will bend inward further rather than buckle under compression. It is also found that the stress-strain curves (Fig. 2b) of APF/STG hybrid foams (APF/2STG, APF/3STG and APF/6STG) still don't have plateau regions. As shown in Fig. 2b, the area of hysteresis loop will become larger as the increase of STG content in APF/STG hybrid foam, reflecting that the energy dissipation capacity would be improved. The calculated energy dissipation of PU, APF, APF/2STG, APF/3STG and APF/6STG at 70 % compression strain is summarized in Fig. 2b. It can be seen that the average energy dissipation value of APF (5.1 kJ/m^3) is 6.4 times higher than that of the original PU foam (0.8 kJ/m^3), and the average energy dissipation value of APF/6STG (19.5 kJ/m^3) can reach to 24.4 times of the original PU foam. This indicates that the incorporation of STG can greatly improve the energy dissipation performance of APF. The high energy-dissipation APF/STG hybrid foam can be widely used for impact protection in the fields of sports, electronics, defense, industry, and aerospace. The drop weight impact system which complies with impact testing standard of ANSI/ISEA 138 is used to evaluate the safeguarding property of the APF/STG hybrid foam (Fig. 2c). A drop hammer with a weight of 2.5 kg is used for the impact test. The samples are placed on the top of anvil and the transmitted force can be measured by the underneath force sensor. The impact energy can be adjusted by the height controller which can determine the height of hammer. As shown in Fig. 2d, under the impact of 10 J, the peak force of APF reaches 19 kN. While for samples APF/2STG, APF/3STG and APF/6STG, the peak forces reduce to 16 kN, 10 kN and 6.8 kN, respectively. It indicates that STF coating on APF attributes to more effective attenuations of impact forces and APF/6STG composite can reduce the peak force by as high as 64 % compared to APF foam. Under higher impact energies of 15 J and 20 J, it is also found that the higher content of STG is, the lower the transmitted force of the APF/STG hybrid foam (Fig. 2e–f). Notably, it is found that the force-time curves of APF, APF/2STG, APF/3STG and APF/6STG show shoulder peak rather than narrow force plot with single peak, which is caused by the auxetic geometry of microstructures of these samples. The broader peaks of force-time curves indicate that the materials can dissipate impact force over a longer timeframe, leading to lower peak force. As shown in Fig. 2g, the impact time of the APF/STG hybrid foams are larger than APF at the same impact energy. For example, under the impact energy of 10 J, the APF/2STG, APF/3STG and APF/6STG present impact time of 2.42 m s, 2.68 m s, 3.33 m s, which is longer than that of APF (2.18 m s). As shown in Fig. 2h, the effect of STG content of the composite has been studied. Under the three impact energies of 10 J, 15 J and 20 J, it is found that the APF/STG hybrid foam could perform better impact protection and low peak force with more STG addition. Furthermore, Fig. 2h also indicates that when the impact energy increases, the difference between the peak force becomes larger, which indicates that APF/STG hybrid foam shows higher energy dissipation under high-rate stimuli. Additionally, we find that the force reduction improvement of the developed APF/STG hybrid foam in this work is much higher than other hybrid auxetic materials reported in literatures [14–16,26,27,37] (Fig. 2i–Table S1). By integrating the auxetic structures with functional materials such as MXene, STF, graphene oxide (GO) and PLA, the highest improvement in peak force reduction can only reach to 39 %. However, with the help of STG as functional additive, the APF/STG hybrid foam shows 64 % more peak force reduction, decreasing the peak force of APF from 19 kN to 6.8 kN. Although Parisi et al. [27] and Wu et al. [37] also used the STG to treat the auxetic polyethylene foam and auxetic Kevlar skeleton, the performances in force reduction were not good, which may be caused by the mismatch of STG content and auxetic structure.

3.3. Dynamic properties and Poisson's ratio of APF/STG hybrid foam

To study the mechanism for the enhanced energy dissipation of APF/STG hybrid foam, the dynamic properties of APF/STG hybrid foam have been investigated by ball rebound tester, dynamic mechanical analysis (DMA) and finite element analysis. In addition, the Poisson's ratios of APF/STG hybrid foams with different STG content under slow compression strain rate (5 mm/min) and high compression strain rate (500 mm/min) have been compared. Fig. 3a is a schematic diagram of the ball rebound tester. A steel ball with diameter of 16 mm is dropped from a given height, and the percentage of rebound height is a measurement of resilience. The high resilience implies the high level of elastic behavior of the material. It can be seen from Fig. 3b that the average resilience of APF/STG hybrid foams is higher than that of APF. For example, APF/6STG has resilience of 27.5 %, which is around two times of that of APF (14.3 %). In addition, the resilience of APF/STG hybrid foam will become larger with the increase of STG content in APF. The result is in accordance with the DMA result as shown in Fig. 3c, which indicates that the higher STG content in APF will result in larger storage modulus especially at higher compressive frequency. The increase of loss modulus of APF/STG hybrid foams (as shown in Fig. 3d) compared to APF is due to the present of STG. Fig. 3e indicates that the loss factor (the ratio of the loss modulus to the storage modulus) values of APF and APF/STG hybrid foam experience decrease-increase process versus the frequency, which is likely due to the synergistic action of rate-dependent property of STG and densification effect of APF. Fig. 3h shows the molecular structures of STG under different compression strain rates which can describe the rate-dependent property of STG. The STG contains several molecular chains and B–O dynamic bonds. When compression stress is applied at a slow rate, molecular chains have enough time to relax and the B–O dynamic bonds are easy to break, thus STG exhibits soft behavior and can be compressed easily. However, under high compression strain rate, the dynamic B–O bond cannot have enough time to break. Therefore, they will lock and hinder the slippage of molecular chains in a short time. Thus, STG becomes stiff and hard to compress. Based on the results of resilience testing and DMA, we can prove that the high storage modulus of STG under high frequency helps APF/STG hybrid foam possess enhanced force attenuation performance. It is interesting to study the effect of STG on the Poisson's ratio of APF/STG hybrid foam since no literature reports this topic at present. The Poisson's ratios of APF/2STG, APF/3STG and APF/6STG are measured under different compression strain rates (5 mm/min and 500 mm/min). As shown in Fig. 3f, under the low compression strain rate of 5 mm/min, the three APF/STG hybrid foams (APF/2STG, APF/3STG and APF/6STG) exhibit a negative Poisson's ratios as low as - 0.2 and still have negative Poisson's ratios at the compression strain of less than 50 %. However, it is notable that the Poisson's ratios of APF/3STG and APF/6STG change to positive values while APF/2STG still have a negative Poisson's ratio under high compression strain rate of 500 mm/min (Fig. 3g). The results indicate that the high STG content in APF will affect the buckling behaviors of cell walls of the foam. To explain the above finding, a simplified model has been built to study the microstructure deformation of APF, APF with low and high content of STF under different compression strain rates, using commercial software ABAQUS. In this simulation, the material performance of PU was described by the Mooney–Rivlin hyperelastic constitutive model. The elasticity of STG was simulated using the isotropic elasticity model with a modulus of elasticity of 0.5 MPa under low compression strain rate and 1000 MPa under high compression strain rate, respectively. The simulation results are presented in Fig. 4. As shown in Fig. 4, for APF, under slow and high compression strain rate, the ribs in the reentrant structures, which are already curved inward, will bend inward further. For APF with low STG content, the ribs will continue to inward even under high compression strain rate since the stiffed STG are still on the surface of ribs and the left part doesn't contact with the right part thus it doesn't provide resistance to affect the movement of ribs. However, for APF with
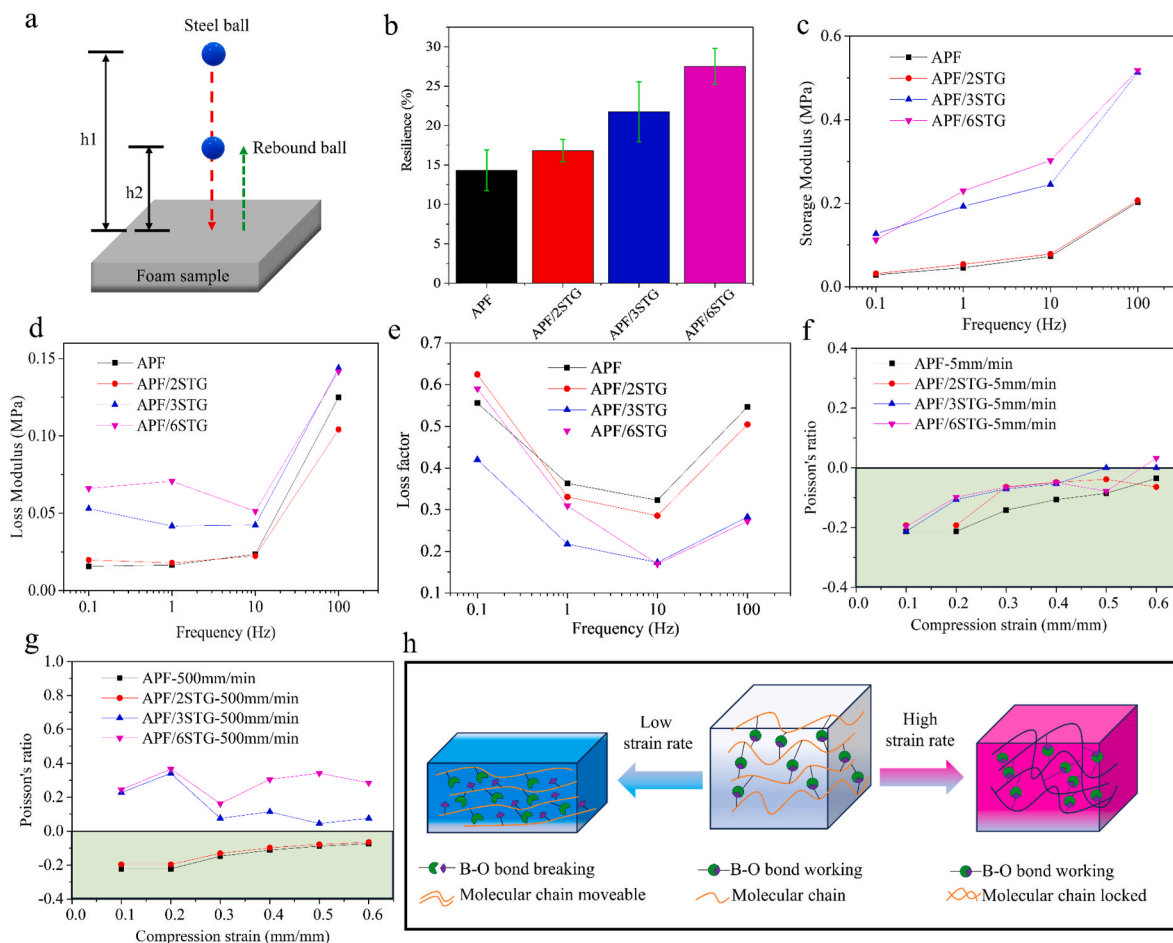
Fig. 3. a) Schematic diagram of ball rebound test. b) Comparison of resilience of APF, APF/2STG, APF/3STG and APF/6STG. c) Storage modulus and d) loss modulus and e) loss factor versus frequency for APF, APF/2STG, APF/3STG and APF/6STG. f-g) Comparison of Poisson's ratio of APF, APF/2STG, APF/3STG and APF/6STG under different compression strain rates. h) Mechanism diagram of shear thickening effect of STG.
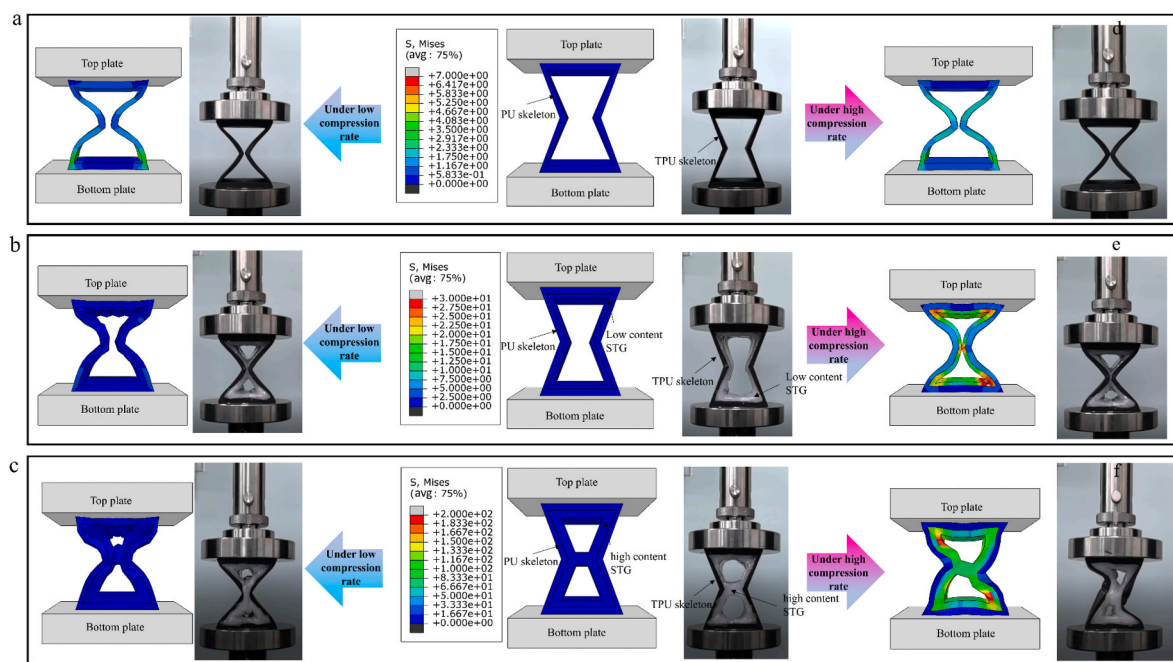

Fig. 4. Experimental and simulated buckling behaviors of cell walls of the PU auxetic structure (a), PU auxetic structure with low STG content (b), and PU auxetic structure with high STG content (c) under different compression strain rates.

high STG content, STG in the left part contacts with the right part. Under low compression strain rate, the STG is in soft state and can flow into the gap of the reentrance structures, thus STG will not affect the inward movement of the ribs. Under high compression strain rate, the STG will become rigid, and it will prevent the ribs from inward thus the composite will lose negative Poisson's ratio effect. The simulation results are further substantiated by experimental data, wherein prototypes with identical dimensions as the simulation models are subjected to diverse compression rates. As demonstrated in Fig. 4, it is observed that the experimental results generate a response that is analogous to that of the finite element models. This finding provides insights to design high energy dissipation materials which have auxetic cell structures and are incorporated with STG. The dimension of auxetic cell structures and the content of STG should be carefully controlled to maximize the synergistic effect of auxetic property and shear thickening property.

3.4. Self-healing behavior of APF/STG hybrid foam

Besides the high energy dissipation performance, the APF/STG hybrid foam is found to have self-healing property. The self-healing process of APF/STG hybrid foam is depicted in Fig. 5a. The sample APF/6STG is cut into two pieces separately. After pressing for a while, the two broken pieces can adhere with each other. The sample after self-healing could withstand a weight without falling apart. As for the tensile test (Fig. 5b), the tensile stress of the self-healed sample with healing process at 120 °C for 1 h is higher than that of self-healed sample at 80 °C and RT. Fig. 5c indicates that the viscosity of STG will decrease greatly

when it is heated at high temperature. The low viscosity of STG and the reversible B–O dynamic bonds in STG will endow APF/STG with good self-healing property. Fig. 5d shows the tensile stress of APF/6STG is around 17.4 kPa after self-healing at 120 °C for 12 h, which means that its mechanical strength recovers around 20 % after healing compared to the pristine APF/6STG. Fig. 5e presents the SEM images of the healed crack area of APF/6STG after undergoing a self-healing process at 120 °C for a duration of 12 h. The images reveal that the STG present in the crack area exhibits a cohesive movement and reattachment to each other, while the APF skeletons remain fractured. Fig. 5f illustrates that the self-healed APF/6STG hybrid foams retain a negative Poisson's ratio as low as −0.2 when subjected to low compression strain rates of 5 mm/min. However, the Poisson's ratios of self-healed APF/6STG change to positive values when exposed to high compression strain rates of 500 mm/min. It is worth noting that the Poisson's ratios of self-healed APF/6STG are slightly reduced when compared to those of APF/6STG before self-healing, as depicted in Figs. 3f and 5f. The APF utilized in APF/6STG is fabricated at a high conversion temperature of 200 °C for 1 h and high volumetric compression ratio of 2.9, and it is expected to exhibit dimensional stability and unchanged Poisson's ratios during the self-healing process at 120 °C, as reported by Duncan et al. [38]. The reduced Poisson's ratios of the self-healed APF/6STG shown in Fig. 5f may be attributed to the more uniform distribution of STG after the self-healing process at 120 °C. This uniform distribution of STG reduces the STG bridges in the APU skeleton, causing the ribs to inward further under compression, ultimately leading to the reduced Poisson's ratios. It is the first time to report the auxetic foam with self-healing property.
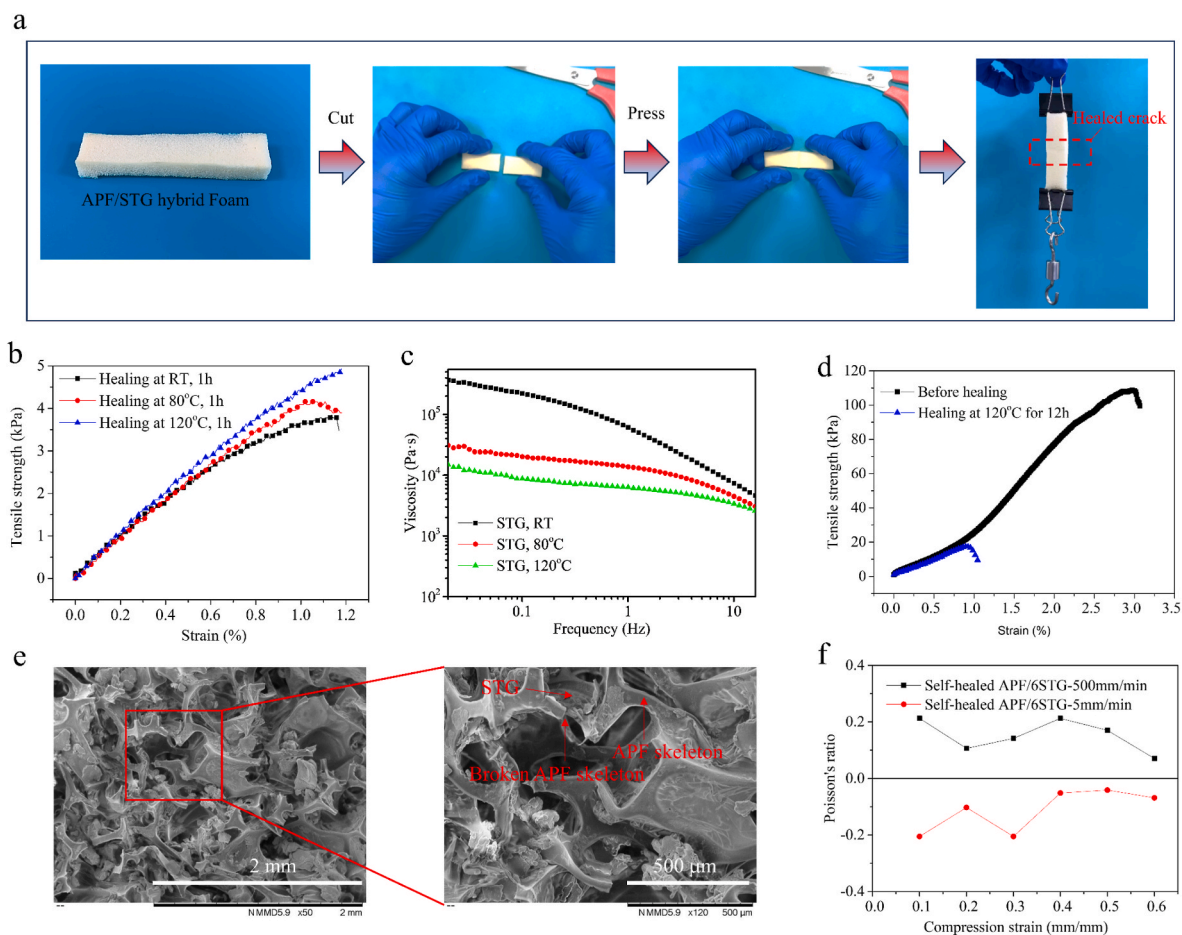

Fig. 5. a) The self-healing process of APF/6STG. b) Tensile stress-strain curves of APF/6STG with healing for 1 h at RT, 80 °C and 120 °C, respectively. c) Viscosity of STG at RT, 80 °C and 120 °C. d) Tensile stress-strain curves of APF/6STG before healing and after healing at 120 °C for 12 h. e) SEM image of the healed crack area of APF/6STG after healing at 120 °C for 12 h. f) Poisson's ratios of APF/6STG after healing at 120 °C for 12 h under different compression strain rates (5 mm/min and 500 mm/min).

The self-healing ability of the APF/STG hybrid foam allows it to repair damage sustained during use. Another benefit is that the self-healable APF/STG can overcome the shape limitation of current auxetic foam. For the reported auxetic foams, they are square or cylindrical shapes due to the production method [10,11,39–46]. It is difficult to make auxetic foam with irregular shapes. By using the self-healing property of the developed APF/STG composite, it can be assembled into structures in any irregular shapes like Lego blocks by its self-healing process.

4. Conclusions

We have successfully developed a novel hybrid auxetic foam that exhibits exceptional energy dissipation performance and possesses a self-healing property. This innovative foam is achieved through the integration of shear thickening gel (STG) with auxetic polyurethane foam (APF). The resulting hybrid auxetic foam demonstrates remarkable anti-impact capacity, as it reduces the peak force by 64 % compared to the pristine APF. To investigate the underlying mechanism behind the enhanced energy dissipation of the APF/STG hybrid foam, we conducted various experiments, including ball rebound testing, Dynamic Mechanical Analysis (DMA), and rate-dependent Poisson's ratio measurement using a high-speed camera. The results indicate that the high storage modulus of STG at high frequencies primarily contributes to the superior energy dissipation observed in the APF/STG hybrid foam. Furthermore, we discovered that careful control of the auxetic cell structures' dimensions and the content of STG is crucial to maximize the synergistic effect between the auxetic and shear thickening properties, resulting in higher energy dissipation materials. Moreover, the developed hybrid auxetic foam exhibits self-healing capabilities, allowing it to repair damage incurred during use. Additionally, its modular nature enables easy assembly, resembling Lego blocks, thereby facilitating the creation of structures in irregular shapes. These remarkable features position the developed hybrid auxetic foam as a promising candidate for the advancement of advanced and intelligent protective materials. Its potential to revolutionize various industrial and commercial applications is undeniable, offering significant opportunities for innovation and improvement in multiple sectors.

CRediT authorship contribution statement

Kang Zhang: Writing – original draft, Methodology, Investigation, Formal analysis, Conceptualization. **Qiang Gao:** Methodology, Formal analysis, Conceptualization. **Jingchao Jiang:** Methodology, Investigation. **Meishan Chan:** Methodology, Data curation. **Xiaoya Zhai:** Methodology, Investigation. **Liuchao Jin:** Methodology, Investigation. **Jiangfan Zhang:** Methodology, Data curation. **Jifan Li:** Resources, Conceptualization. **Wei-Hsin Liao:** Writing – review & editing, Supervision, Resources, Investigation.

Declaration of competing interest

The authors declare that they have no known competing financial interests or personal relationships that could have appeared to influence the work reported in this paper.

Data availability

Data will be made available on request.

Acknowledgements

Appendix A. Supplementary data

Supplementary data to this article can be found online at https://doi.org/10.1016/j.compscitech.2024.110475.

References

[1] J. Huang, Y.C. Xu, S.H. Qi, J.J. Zhou, W. Shi, T.Y. Zhao, M.J. Liu, Ultrahigh energy-dissipation elastomers by precisely tailoring the relaxation of confined polymer fluids, Nat. Commun. 12 (2021) 3610, https://doi.org/10.1038/s41467-021-23984-2.

[2] J.B. Chen, E. Li, W.Y. Liu, Y.Q. Mao, S.J. Hou, Sustainable composites with ultrahigh energy absorption from beverage cans and polyurethane foam, Compos. Sci. Technol. 239 (2023) 110047, https://doi.org/10.1016/j.compscitech.2023.110047.

[3] J.K. Gan, F.L. Li, K.Q. Li, E. Li, B. Li, Dynamic failure of 3D printed negative-stiffness meta-sandwich structures under repeated impact loadings, Compos. Sci. Technol. 234 (2023) 109928, https://doi.org/10.1016/j.compscitech.2023.109928.

[4] Y.Z. Chen, L.H. Jin, Reusable energy-absorbing architected materials harnessing snapping-back buckling of wide hyperelastic columns, Adv. Funct. Mater. 31 (31) (2021) 2102113, https://doi.org/10.1002/adfm.202102113.

[5] K. Zhang, X.Y. Zhang, Q. Gao, M.S. Chan, S.L. Zhang, J.F. Li, W.H. Liao, Ultrahigh energy-dissipation and multifunctional auxetic polymeric foam inspired by balloon art, Compos. Appl. Sci. Manuf. 167 (2023) 107435, https://doi.org/10.1016/j.compositesa.2023.107435.

[6] M. Tomin, Á. Kmetty, Polymer foams as advanced energy absorbing materials for sports applications - a review, J. Appl. Polym. Sci. 139 (9) (2022) 51714, https://doi.org/10.1002/app.51714.

[7] M. Tang, G. Huang, H.H. Zhang, Y.L. Liu, H.J. Chang, H.Z. Song, D.H. Xu, Z.G. Wang, Dependences of rheological and compression mechanical properties on cellular structures for impact-protective materials, ACS Omega 2 (5) (2017) 2214–2223, https://doi.org/10.1021/acsomega.7b00242.

[8] M.H.N. Pour, G. Payganeh, M. Tajdari, Experimental and numerical study on the mechanical behavior of 3D printed re-entrant auxetic structure filled with carbon nanotubes- reinforced polymethylmethacrylate foam, Mater. Today Commun. 34 (2023) 104936, https://doi.org/10.1016/j.mtcomm.2022.104936.

[9] J.Q. Wu, X. Chen, H.Y. Zhu, P. Wang, F.N. Jin, H.L. Fan, Meta-honeycomb sandwich tubes: designing, manufacturing, and crashworthiness performance, Compos. Sci. Technol. 240 (2023) 110096, https://doi.org/10.1016/j.compscitech.2023.110096.

[10] M. Bianchi, F.L. Scarpa, C.W. Smith, Stiffness and energy dissipation in polyurethane auxetic foams, J. Mater. Sci. 43 (2008) 5851, https://doi.org/10.1007/s10853-008-2841-5.

[11] O. Duncan, L. Foster, T. Senior, A. Alderson, T. Allen, Quasi-static characterization and impact testing of auxetic foam for sports safety applications, Smart Mater. Struct. 25 (2016) 054014, https://doi.org/10.1088/0964-1726/25/5/054014.

[12] T.C. Lim, A. Alderson, K.L. Alderson, Experimental studies on the impact properties of auxetic materials, Phys. Status Solidi B 251 (2) (2014) 307–313, https://doi.org/10.1002/pssb.201384249.

[13] D. Fan, Z. Shi, N. Li, J. Qiu, H.P. Xing, Z.W. Jiang, M.G. Li, T. Tang, Novel method for preparing a high-performance auxetic foam directly from polymer resin by a one- pot CO$_2$ foaming process, ACS Appl. Mater. Interfaces 12 (2020) 48040, https://doi.org/10.1021/acsami.0c15383.

[14] E. Kim, H.M. Zhang, J.H. Lee, H.M. Chen, H. Zhang, M.H. Javed, X. Shen, J.K. Kim, MXene/polyurethane auxetic composite foam for electromagnetic interference shielding and impact attenuation, Compos. Appl. Sci. Manuf. 147 (2021) 106430, https://doi.org/10.1016/j.compositesa.2021.106430.

[15] J.H. Oh, J.S. Kim, V.H. Nguyen, I.K. Oh, Auxetic graphene oxide-porous foam for acoustic wave and shock energy dissipation, Compos. B Eng. 186 (2020) 107817, https://doi.org/10.1016/j.compositesb.2020.107817.

[16] J.S. Kim, M. Mahato, J.H. Oh, I.K. Oh, Multi-purpose auxetic foam with honeycomb concave micropattern for sound and shock energy absorbers, Adv. Mater. Interfac. 10 (4) (2023) 2202092, https://doi.org/10.1002/admi.202202092.

[17] M.H. Wei, K. Lin, L. Sun, Shear thickening fluids and their applications, Mater. Des. 216 (2022) 110570, https://doi.org/10.1016/j.matdes.2022.110570.

[18] B. Liu, C.B. Du, H.X. Deng, Z.Y. Fan, J.S. Zhang, F. Zeng, Y.K. Fu, X.L. Gong, Mechanical properties of magneto-sensitive shear thickening fluid absorber and application potential in a vehicle, Compos. Appl. Sci. Manuf. 154 (2022) 106782, https://doi.org/10.1016/j.compositesa.2021.106782.

[19] B. Liu, C.B. Du, L.Y. Wang, Y.K. Fu, L. Song, The rheological properties of multifunctional shear thickening materials and their application in vehicle shock absorbers, Smart Mater. Struct. 30 (8) (2021) 085028, https://doi.org/10.1088/1361-665X/ac0d10.

[20] Z.Y. Fan, L. Lu, M. Sang, J.P. Wu, X.Y. Wang, F. Xu, X.L. Gong, T.Z. Luo, K.C.F. Leung, S.H. Xuan, Wearable safeguarding leather composite with excellent sensing, thermal management, and electromagnetic interference shielding, Adv. Sci. (2023) 2302412, https://doi.org/10.1002/advs.202302412.

[21] J.S. Zhang, Y. Wang, J.Y. Zhou, J.P. Wu, S. Liu, M. Sang, B. Liu, Y.C. Pan, X.L. Gong, Multi-functional STF-based yarn for human protection and wearable systems, J. Chem. Eng. 453 (2023) 139869, https://doi.org/10.1016/j.cej.2022.139869.

[22] B. Liu, C.B. Du, H.X. Deng, Y.K. Fu, F. Guo, L. Song, X.L. Gong, Study on the shear thickening mechanism of multifunctional shear thickening gel and its energy

dissipation under impact load, Polymer 247 (2022) 124800, https://doi.org/10.1016/j.polymer.2022.124800.

[23] Q.Y. He, S.S. Cao, Y.P. Wang, S.H. Xuan, P.F. Wang, X.L. Gong, Impact resistance of shear thickening fluid/Kevlar composite treated with shear-stiffening gel, Compos. Appl. Sci. Manuf. 106 (2018) 82–90, https://doi.org/10.1016/j.compositesa.2017.12.019.

[24] H. Tu, P.Z. Xu, Z. Yang, F. Tang, C. Dong, Y.C. Chen, W.J. Cao, C.G. Huang, Y. C. Guo, Y.P. Wei, Effect of shear thickening gel on microstructure and impact resistance of ethylene–vinyl acetate foam, Compos. Struct. 311 (2023) 116811, https://doi.org/10.1016/j.compstruct.2023.116811.

[25] G.J. Lin, J.Q. Li, F. Li, P.W. Chen, W.F. Sun, Low-velocity impact response of sandwich composite panels with shear thickening gel filled honeycomb cores, Compos. Commun. 32 (2022) 101136, https://doi.org/10.1016/j.coco.2022.101136.

[26] P. Nakonieczna, Ł. Wierzbicki, B. Sladowska, M. Leonowicz, J. Lisiecki, D. Nowakowski, Composites with impact absorption ability based on shear thickening fluids and auxetic foams, Compos. Theory Pract. 2 (2017) 67–72.

[27] M. Parisi, T. Allen, M. Colonna, N. Pugno, O. Duncan, Indentation and impact response of conventional, auxetic, and shear thickening gel infused auxetic closed cell foam, Smart Mater. Struct. 32 (7) (2023) 074004, https://doi.org/10.1088/1361-665X/acd91c.

[28] S.Y. Wang, W.U. Marek, Self-healing polymers, Nat. Rev. Mater. 5 (8) (2020) 562–583, https://doi.org/10.1038/s41578-020-0202-4.

[29] J.F. Patrick, N.R. Sottos, S.R. White, Microvascular based self-healing polymeric foam, Polymer 53 (19) (2012) 4231–4240, https://doi.org/10.1016/j.polymer.2012.07.021.

[30] S.Z. Cao, W. Zhu, T. Liu, Bio-inspired self-healing polymer foams with bilayered capsule Systems, Compos. Sci. Technol. 195 (2020) 108189, https://doi.org/10.1016/j.compscitech.2020.108189.

[31] X.F. Zhao, J. H Zhang, A novel composite silicone foam with enhanced safeguarding performance and self-healing property, React. Funct. Polym. 138 (2019) 114–121, https://doi.org/10.1016/j.reactfunctpolym.2019.03.004.

[32] Z. Yu, C. Wang, X. Zhang, A.D. Phule, Y.X. Zhao, S.B. Wen, Z.X. Zhang, Self-healing performance of lightweight and electrically conductive ethylene-vinyl acetate copolymer/carbon nanotubes composite foam, Compos. Commun. 29 (2022) 101051, https://doi.org/10.1016/j.coco.2021.101051.

[33] Q.C. Zhang, W.J. Lu, F. Scarpa, D. Barton, K. Rankin, Y.P. Zhu, Z.Q. Lang, H. X. Peng, Topological characteristics and mechanical properties of uniaxially thermoformed auxetic foam, Mater. Des. 211 (2021) 110139, https://doi.org/10.1016/j.matdes.2021.110139.

[34] S. Liu, S. Wang, M. Sang, J.Y. Zhou, J.S. Zhang, S.H. Xuan, X.L. Gong, Nacre-mimetic hierarchical architecture in polyborosiloxane composites for synergistically enhanced impact resistance and ultra-efficient electromagnetic

interference shielding, ACS Nano 16 (11) (2022) 19067–19086, https://doi.org/10.1021/acsnano.2c08104.

[35] W.J. Lu, Q.C. Zhang, F.X. Qin, P. Xu, Q. Chen, H. Wang, F. Scarpa, H.X. Peng, Hierarchical network structural composites for extraordinary energy dissipation inspired by the cat paw, Appl. Mater. Today 25 (2021) 101222, https://doi.org/10.1016/j.apmt.2021.101222.

[36] D.W. Li, X.C. Bu, Z.P. Xu, Y.W. Luo, H. Bai, Bioinspired multifunctional cellular plastics with a negative Poisson's ratio for high energy dissipation, Adv. Mater. 32 (33) (2020) 2001222, https://doi.org/10.1002/adma.202001222.

[37] L. Wu, F. Zhao, Z. Lu, J.H. Lin, Q. Jiang, Impact energy absorption composites with shear stiffening gel-filled negative Poisson's ratio skeleton by kirigami method, Compos. Struct. 298 (2022) 116009, https://doi.org/10.1016/j.compstruct.2022.116009.

[38] O. Duncan, F. Clegg, A. Essa, A.M.T. Bell, L. Foster, T. Allen, A. Alderson, Effects of heat exposure and volumetric compression on Poisson's ratios, Young's moduli, and polymeric composition during thermo-mechanical conversion of auxetic open cell polyurethane foam, Phys. Status Solidi B 256 (1) (2018) 1800393, https://doi.org/10.1002/pssb.201800393.

[39] R. Lakes, Foam structures with a negative Poisson's ratio, Science 235 (1987) 1038, https://doi.org/10.1126/science.235.4792.1038.

[40] S. Mohsenizadeh, Z. Ahmad, R. Alipour, R.A. Majid, Y. Prawoto, Quasi tri-axial method for the fabrication of optimized polyurethane auxetic foams, Phys. Status Solidi B 256 (2009) 1800587, https://doi.org/10.1002/pssb.201800587.

[41] R. Critchley, V. Smy, I. Corni, J.A. Wharton, F.C. Walsh, R.J.K. Wood, K.R. Stokes, Experimental and computation assessment of thermomechanical effects during auxetic foam fabrication, Sci. Rep. 10 (1) (2020) 1–14, https://doi.org/10.1038/s41598-020-75298-w.

[42] T. Allen, T. Hewage, C. Newton-Mann, W.Z. Wang, O. Duncan, A. Alderson, Fabrication of auxetic foam sheets for sports applications, Phys. Status Solidi B 254 (12) (2017) 1700596, https://doi.org/10.1002/pssb.201700596.

[43] Y.T. Yao, Y. Luo, Y.C. Xu, B. Wang, J.Y. Li, H. Deng, H.B. Lu, Fabrication and characterization of auxetic shape memory composite foams, Compos. B Eng. 152 (2018) 1–7, https://doi.org/10.1016/j.compositesb.2018.06.027.

[44] O. Duncan, G. Leslie, S. Moyle, D. Sawtell, T. Allen, Developments on auxetic closed cell foam pressure vessel fabrications, Smart Mater. Struct. 31 (7) (2022) 074002, https://doi.org/10.1088/1361-665X/ac6ea2.

[45] W. Jiang, X. Ren, S.L. Wang, X.G. Zhang, X.Y. Zhang, C. Luo, Y.M. Xie, F. Scarpa, A. Alderson, K.E. Evans, Manufacturing, characteristics and applications of auxetic foams: a state-of-the-art review, Compos. B Eng. 235 (2022) 109733, https://doi.org/10.1016/j.compositesb.2022.109733.

[46] Q.C. Zhang, F. Scarpa, D. Barton, Y.P. Zhu, Z.Q. Lang, D.Y. Zhang, H.X. Peng, Impact properties of uniaxially thermoformed auxetic foams, Int. J. Impact Eng. 163 (2022) 104176, https://doi.org/10.1016/j.ijimpeng.2022.104176.